




**Temperature-induced gradual polymorphic structural crossover in liquid indium, tin, and antimony**Q. L. Shi <sup>1</sup>, X. D. Wang <sup>1,\*</sup>, Q. P. Cao,<sup>1</sup> S. Q. Ding,<sup>1</sup> D. X. Zhang,<sup>1,2</sup> K. A. Beyer <sup>3</sup> and J. Z. Jiang<sup>1,†</sup><sup>1</sup>*International Center for New-Structured Materials (ICNSM), State Key Laboratory of Silicon Materials, and School of Materials Science and Engineering, Zhejiang University, Hangzhou 310027, China*<sup>2</sup>*State Key Laboratory of Modern Optical Instrumentation, Zhejiang University, Hangzhou 310027, People's Republic of China*<sup>3</sup>*X-Ray Science Division, Advanced Photon Source, Argonne National Laboratory, Argonne, Lemont, Illinois 60439, USA*

(Received 2 June 2023; revised 21 December 2023; accepted 11 January 2024; published 26 January 2024)

Temperature-induced polymorphic structural crossover in metallic liquid indium (In), tin (Sn), and antimony (Sb) is investigated by *in situ* high-energy x-ray diffraction and *ab initio* molecular dynamics simulations. The results demonstrate the existence of a temperature-induced reversible and gradual structural crossover in these three liquids, reflecting from both “static” structures, e.g., peak positions of the structure factor and pair distribution function, bond angle distribution, number of tetrahedra, cluster connection, free volume, and dynamical behaviors, including the relaxation time, diffusion coefficient, and non-Gaussian parameter. The main difference from liquid In, Sn, to Sb is that not only the large-sized free volume but also the anharmonicity and the dynamical heterogeneity increase significantly with the appearance of strong covalent bonds. These findings will deepen the understanding of liquid structure and the liquid-liquid transition in metallic liquids.

DOI: [10.1103/PhysRevB.109.024112](https://doi.org/10.1103/PhysRevB.109.024112)**I. INTRODUCTION**

Temperature-induced structural transition in metallic liquids has been a long-standing issue of great interest in materials science and condensed matter physics. In strongly covalent elements, a density-related first-order liquid-liquid phase transition has been reported in the supercooled liquid Si [1,2], and the pressure-induced phase transition in liquid Ge [3,4], which were accompanied with the significant change in the nearest coordination number. On the other hand, the liquid-to-liquid crossover is also a common structural evolution phenomenon that occurs in metallic liquids. Here we defined the term “a gradual polymorphic structural crossover” to be a phenomenon that has progressive changes in structure and properties but no change in the chemical composition. With the help of modern techniques, such as high-energy synchrotron x-ray based techniques, levitation, and *ab initio* molecular dynamics (AIMD) simulations [5], the insight on the structure of metallic liquids has entered a new perspective. Although the structural transition has been reported in various metallic liquids, from pure Rb [6], Ce [7], Ga [8–10], to binary Ga-In [11], Ag-Ga [12], Sn-Zn [13], and to multicomponent La-Al-Ni [14], Pd-Ni-P [15], and  $Zr_{41.2}Ti_{13.8}Cu_{12.5}Ni_{10}Be_{22.5}$  [16], no general picture of how the structural evolution happens in metallic liquids has been established yet. In terms of “static” structure changes of pure element liquids, Lou *et al.* [17] observed the “negative expansion” of interatomic distances in the first shell in metallic liquids with increasing temperature, resulting from the temperature-induced evolution of high-coordinated polyhedra into low-coordinated

ones. Various trends of structural evolution for the second- and third-coordinated shells were also reported [18,19]. By utilizing synchrotron x-ray diffraction and dynamic simulations, Georgarakis *et al.* [20] discovered that within the undercooled liquid region the Zr-Cu-Al liquid undergoes fast structural rearrangements, significantly enhancing its short- and medium-range order. In terms of the dynamical behavior of Cu-Zr-Al liquid, Zhang and co-workers [21,22] described an increase in spatially heterogeneous dynamics arising from strong dynamic decoupling below the crossover temperature  $T_A$  (approximately twice  $T_g$ ). The dynamic crossover in the viscosity of different supercooled liquids was also observed in the earlier reports [23,24]. These reported results suggest that not only the averaged static structure but also the dynamical behavior should be considered to reveal the liquid structural evolution in studies. Due to complicated many-body interactions in multicomponent metallic liquids, the combination studies on structure and dynamics for single element series, which are still missing, become even more preferable to simplify such interactions.

Three elements, indium (In), tin (Sn), and antimony (Sb), are next to each other in the fifth cycle of the periodic table with melting points of about 431.1, 505.1, and 903.8 K, respectively. The low melting point makes In widely studied in the liquid state [25–30]. For example, it was reported that the liquid In had “closest packing” and could be approximated by the hard sphere model [25]. The viscosity of liquid In decreased with increasing temperature basically in an exponential relationship, in which a sudden change was observed at around 700 K [27]. Mudry *et al.* [30] used x-ray diffraction and the reverse Monte Carlo method to study the structural transition of liquid In within a wide temperature range. Below and above 640 K, they found that the first main peak position of  $S(q)$ , interatomic spacing, thermal expansion coefficient, and the coordination number of the nearest neighbors showed different temperature dependences. The liquid

\*Author to whom correspondence should be addressed: wangxd@zju.edu.cn

†Author to whom correspondence should be addressed: jiangjz@zju.edu.cn

Sn has a complex atomic packing structure [31–42], likely containing two atomic arrangements in the liquid state. Thus, a double hard sphere model was proposed to describe its liquid structure [31,32], and was supported by Itami *et al.* [35] and Calderín *et al.* [37] using neutron diffraction and AIMD simulations. By calculating the bond angle distribution function, they found that the tetrahedra remained in the liquid even at high temperatures. Through the viscosity, it was found that the liquid Sn had two kinks near 693 and 1093 K [36] or 673 and 1073 K [38], but the resistivity only showed a kink near 673 K [39]. Xu *et al.* revealed strong covalent interactions in liquid Sn at high temperatures through the use of high-energy synchrotron radiation and AIMD simulations under the NPH ensemble [42]. The Sb has the properties of semimetals [43–49]. Double structures were suggested in liquid Sb through the study of the shoulder peak of structure factor [43]. From the resistivity of liquid Sb, an abnormal mutation was found at about 995 K [44]. The x-ray absorption fine structure indicated that the liquid Sb could retain the local structural arrangement and the Peierls distortion in the initial stage of melting [46], which disappeared at around 1023 K with increasing temperature. Also, AIMD simulations [47] showed that the liquid Sb had abnormal structural changes near 1023 K by studying the temperature dependence of structure factor, coordination number, bond angle distribution function, and bond orientation parameters  $Q_4$  and  $Q_6$ . Jones *et al.* [48] combined density functional and molecular dynamics calculations and found the presence of collective excitations and three short covalent bonds in  $Sb_n$  clusters.

The fact is that in previous reported studies, different mechanisms had been suggested due to the availability of only a few temperature points with a large temperature step of, e.g., 200 K, even 300 K, and relatively poor quality of experimental data. Thus, it is reasonable to conclude that these suggested microscopic mechanisms for observed structural changes remain unconvincing. To dig the exact origin for structural crossover in liquid In, Sn, and Sb, it is essential to record high-quality experimental data with many more temperature points, i.e., a much smaller temperature step, e.g., 2–5 K, which are still missing. By using high-energy *in situ* synchrotron radiation x-ray diffraction and AIMD simulations, we here systematically studied the liquid structure of these three elements through the analyses of structure factor, pair distribution function, bond angle distribution, number of tetrahedra, cluster connection, free volume, diffusion coefficient, intermediate scattering function, and non-Gaussian parameter. The results demonstrated that the structural crossovers indeed gradually happen in liquid In, Sn, and Sb within the measured temperature ranges, which are highly correlated with their inside differences in tetrahedral clusters, cluster connection, large-sized free volume content, strength of covalent bonds, and anharmonicity.

## II. EXPERIMENTAL AND SIMULATION METHODS

High-purity (99.99%) In, Sn, and Sb rods were filled into thin-walled (thickness of 0.01 mm) capillaries with 1.5 mm in diameter. The capillaries with samples inside were then vacuum-sealed at about  $4.6 \times 10^{-4}$  Pa and then placed at the center of a heating furnace (Linkam TS1500). When the

sample was continuously heated/cooled at a rate of 10 K/min, the diffraction patterns were recorded by a flat-panel Si detector (Perkin-Elmer 1621) with  $200 \times 200 \text{ mm}^2$  pixel size and  $2048 \times 2048$  pixels at the 11-ID-C of Advanced Photon Source (APS), Chicago. A  $\text{CeO}_2$  standard sample was used to measure the sample-to-detector distance. The wavelength used was about 0.1173 Å and the beam size was  $0.3 \times 0.3 \text{ mm}^2$ . The incident beam flux was recorded for intensity normalization. The exposure time was 1 s and every 20 patterns were summed to output one diffraction data. The temperature interval between two high-energy x-ray diffraction (HEXRD) patterns is about 3 K. The liquid In was first heated from 453 to 1273 K and then continued to cool down to 453 K. The liquid Sn was heated from 503 to 1263 K and then cooled down to 503 K, while the liquid Sb was heated from 1023 to 1373 K and then down to 921 K. Scattering intensities  $I(q)$  were integrated under the software package FIT2D [50], from which the experimental structure factors  $S(q)$  were derived by subtracting the appropriate background and correcting for oblique incidence, absorption, sample geometry, multiple scattering, fluorescence, and Compton scattering contributions using the programs PDFGETX2 [51] and GSASII [52].

*Ab initio* molecular dynamics simulations of metallic liquids were undertaken by using the Vienna *ab initio* simulation package (VASP) [53]. The simulations were performed with the canonical *NVT* ensemble (constant number, volume, and temperature), and the temperature was controlled by the Nose-Hoover thermostat [54,55]. Only the  $\Gamma$  point was considered to sample the Brillouin zone in simulations since the cell box was sufficiently large. The interaction between electrons and ions was modeled by a projector augmented-wave method [56]. The general gradient approximation (GGA) in the form by Pedrew-Burke-Ernzerhof (PBE) was used for the exchange-correlation energy functional [57]. A typical time interval of 3 fs was applied with the Verlet algorithm to integrate Newton's equations of motion. Firstly, a cubic cell with periodic boundary conditions was constructed by means of the crystal configuration, where the cell box of In and Sn includes 250 atoms, and of Sb includes 200 atoms. Secondly, each cell was fully melted at 2000 K to eliminate the original periodicity. Then, it was cooled at a cooling rate of  $3.33 \times 10^{13}$  K/s. The pressure was adjusted at each selected temperature and maintained within  $\pm 0.5$  kbar during the isothermal relaxation. The temperature ranges for liquid In and Sn are 400–1500 K and 500–1500 K, respectively, while 10 000 configurations are reserved at the temperatures every 100 K. The temperature range for liquid Sb is 700–1700 K with 6000 relaxed configurations being reserved every 100 K. Moreover, the  $r^2$ scan meta-generalized gradient approximation [58] for liquid Sb in AIMD and the modified embedded atom method (MEAM) potentials for liquid In and Sn in classic molecular dynamics (MD) were conducted to verify the reliability of our theoretical calculations.

## III. RESULTS AND DISCUSSION

### A. Static structure analyses by *in situ* HEXRD experiments

Based on the HEXRD results, the structure factor  $S(q)$  and pair distribution function  $G(r)$  of three metallic liquids have

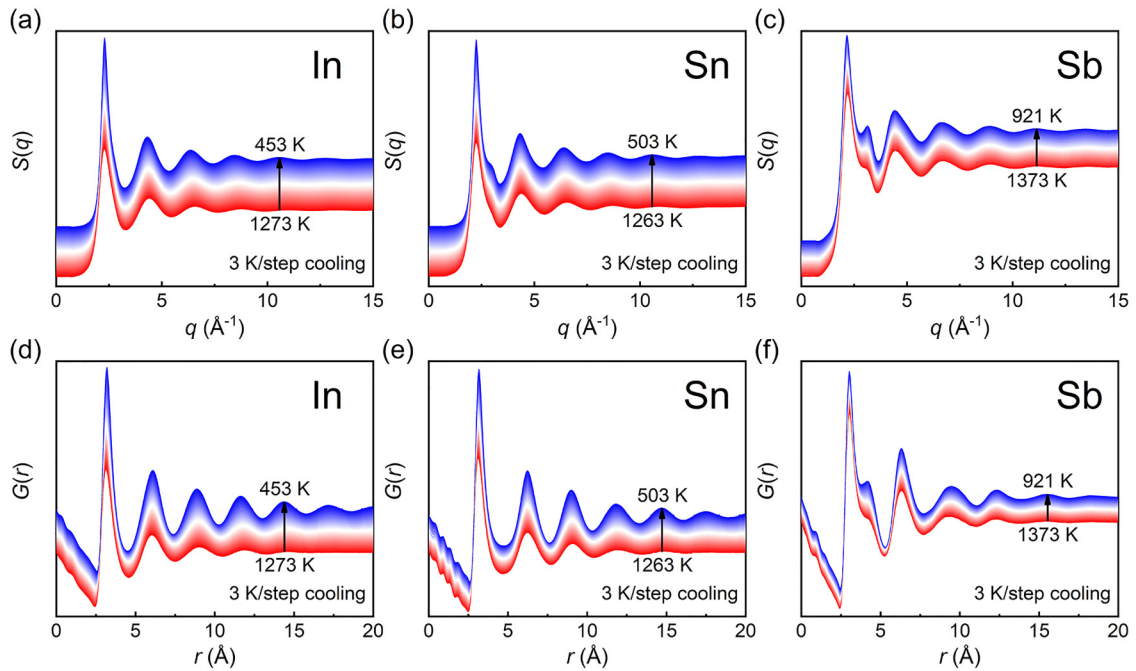


FIG. 1. The structure factor and pair distribution function for liquid In (a), (d), Sn (b), (e), and Sb (c), (f) measured by HEXRD upon cooling at a rate of 10 K/min.

been obtained to characterize their liquid structures. The structure factor describes the contribution of atomic structure and species to scattering intensity in disordered systems and can be measured by x-ray scattering experiments using Eq. (1):

$$S(q) = \frac{I(q) - \langle f^2(q) \rangle - K}{\langle f(q) \rangle^2}, \quad (1)$$

where  $I(q)$  is the diffraction intensity,  $f(q)$  is the atomic scattering factor,  $K$  is the Compton inelastic scattering parameter, and  $q$  is the scattering vector. And  $q_{\max} = 20 \text{ \AA}^{-1}$  is chosen.

Taking the Fourier transform of the structure factor, one can obtain the pair distribution function (PDF) [59], which describes the probability distribution along the distance between paired atoms in a given system, as presented in Eq. (2):

$$G(r) = \frac{2}{\pi} \int_0^{\infty} [S(q) - 1] \sin(qr) q dq \quad (2)$$

The structure factors and pair distribution functions of liquid In, Sn, and Sb in the cooling process are shown in Fig. 1 and those during the heating process are shown in Fig. S1 in the Supplemental Material [60]. From  $S(q)$  curves, one can see that a shoulder peak on the right side of the first main peak is gradually getting more pronounced from In to Sn and Sb with decreasing temperature, indicating that the higher ordering remains in liquid Sb than in liquid Sn and In. This can also be demonstrated from the shoulder peak at the large  $r$  side of the first main peak in the  $G(r)$  curve of liquid Sb, showing the existence of two Sb-Sb atomic distances ( $\sim 3.3$  and  $4.3 \text{ \AA}$ ) within the first shell although the shoulder intensity becomes decreased at high temperatures.

The peak positions of the  $S(q)$  and  $G(r)$  curves are often used to reflect how the atomic structure changes in metallic

liquids [61,62]. According to the symmetry of peak profiles, two Gaussian peaks were used to fit the first peak, and one to fit the second and third peaks. Figures 2 and 3 show the changes in the first three peak positions in  $S(q)$  and  $G(r)$  of these three liquids, respectively. The first three peak positions in  $S(q)$  and  $G(r)$  have similar variation trends with temperature for liquid In and Sn, but have some differences from those of liquid Sb. Figures 2(a) and 2(b) show that the  $q_1$  in  $S(q)$  of liquid In and Sn decreases whereas  $q_2$  and  $q_3$  increase with rising temperature. Inversely, as shown in Figs. 3(a) and 3(b), the  $r_1$  and  $r_2$  in  $G(r)$  of both liquids just decrease and  $r_3$  increases with increasing temperature. When looking at the liquid Sb in Fig. 2(c), we found that it exhibits an opposite behavior of  $q_1$  in  $S(q)$  compared with liquid In and Sn, i.e., it increases with temperature rising, which means that the liquid Sb may have some structural shrinking on the medium-range scale. As seen in Fig. 3(c), the  $r_2$  and  $r_3$  in  $G(r)$  of liquid Sb indeed decrease with rising temperature. However, the  $r_1$  value in  $G(r)$  exhibits a kind of nonmonotonic behavior with temperature, i.e., it firstly increases to a maximum at the crossover temperature and then decreases with rising temperature. Such peak shifting behavior is quite distinct from that of liquid In and Sn and may depend on its specific local shoulder peak in  $G(r)$ , as shown in Fig. 1(f). Comparing to  $G(r)$ ,  $g(r)^*r$  has a more explicit physical meaning, which presents the fluctuation part of the radial distribution function around its average distribution. As shown in Fig. S2, the first peak positions in  $g(r)^*r$  exhibit a similar feature and trend with those in  $G(r)$  for three liquids although the peak position values are little different. In addition, we also analyzed the mass centers and heights of the first three peaks in  $S(q)$  and  $G(r)$  (see Figs. S3–S6), which also support the peak position results above, showing the different structural changes in liquid Sb. All the curves on heating and cooling are well overlapped with each other,

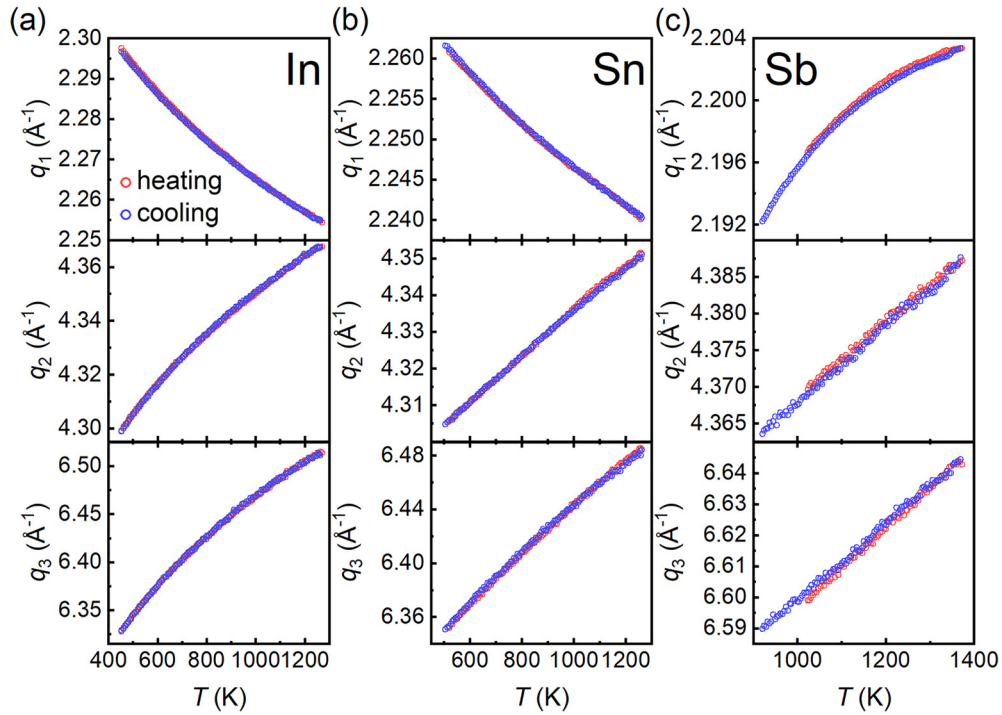


FIG. 2. From top to bottom, the peak positions for the first three peaks on  $S(q)$  of liquid In (a), Sn (b), and Sb (c) as a function of temperature. The red circle represents the heating process, and the blue circle represents the cooling. The following is the same.

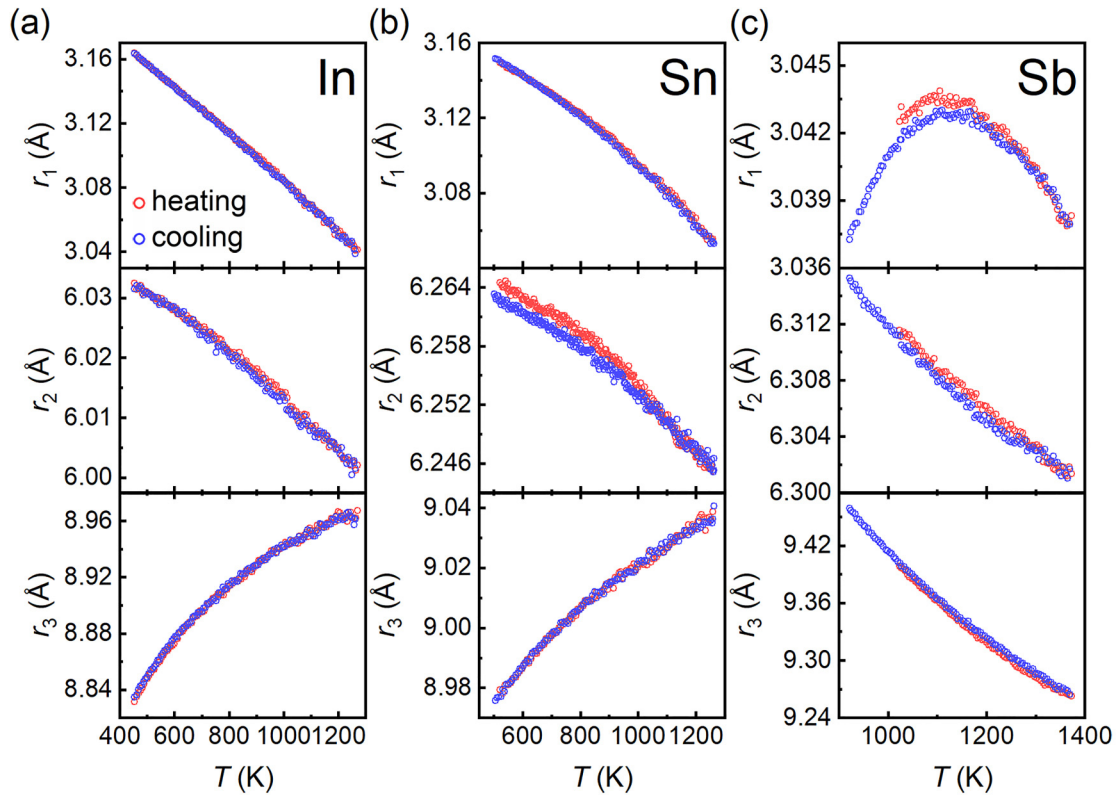


FIG. 3. From top to bottom, the peak positions of the first three peaks on  $G(r)$  for liquid In (a), Sn (b), and Sb (c) as a function of temperature.



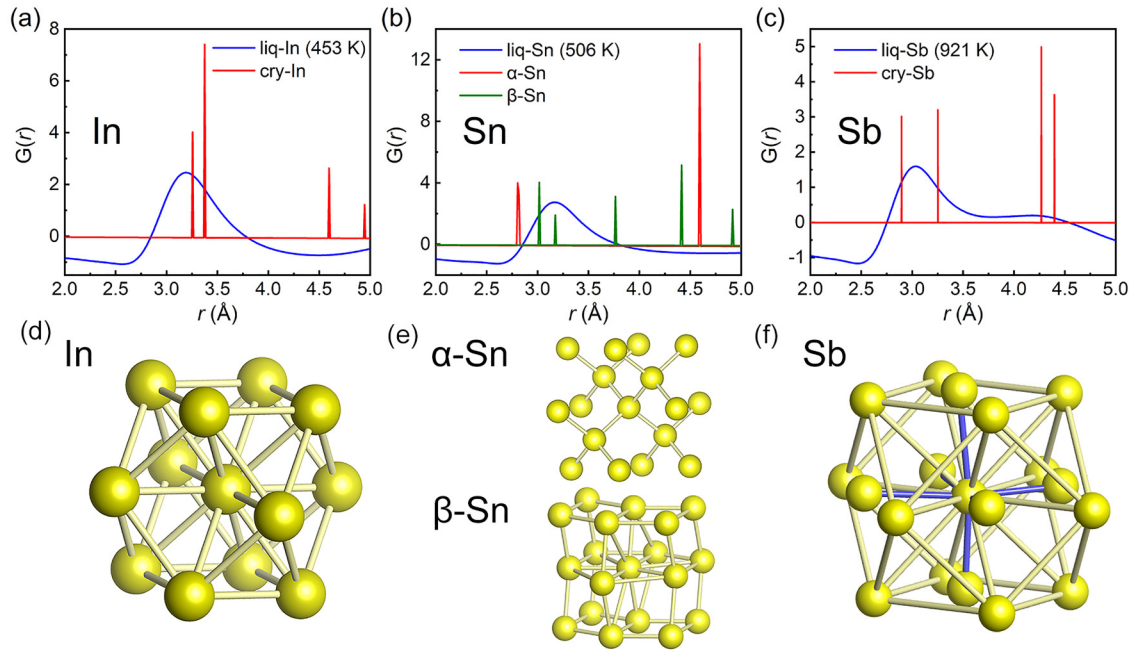


FIG. 4. Pair distribution function of crystal and liquid In (a), Sn (b), and Sb (c). Typical cluster model found in the crystal In (d), Sn (e), and Sb (f).

indicating that the gradual structural crossovers are reversible in three liquids.

### B. Static structure analyses by AIMD simulations

To understand the above experimental results, i.e., how the structural changes happen in metallic liquids at the atomic scale, we performed AIMD simulations for these three liquids. The structure factor and pair distribution function of each liquid created by AIMD agree with the experimental results (see Fig. S7). The results are better for liquid In, and gradually worsen for liquid Sn and Sb, which is possibly due to the less degree of structural heterogeneities under the higher cooling rate. We confirmed that the temperature-dependent peak positions deduced by calculations can still represent the atomic arrangements to a certain extent (see Fig. S8), exhibiting similar variation trends with the experimental data. Thus, we believe that although some inconsistency exists between simulation and experimental data, e.g., the peak shape of the calculated  $S(q)$  and  $G(r)$  cannot be fully matched with experimental data, the obtained atomic configurations are reliable and could be used for further local atomic structure analyses.

#### 1. Pair distribution function and crystalline model

The liquid comes from the melting of its crystalline phase, which might inherit some local atomic packing structure of its mother phase. Hence, we compared the PDF profiles of liquid In, Sn, and Sb at the temperatures near above their melting points with those of their crystals, as shown in Figs. 4(a), 4(b), and 4(c), respectively. Figures 4(d), 4(e), and 4(f) show the cluster models composed of the nearest neighboring atoms in ideal crystals of three metals, respectively. It is clear that the solid In locally has both tetrahedral and half-octahedral structures with bond lengths of 3.2 and 3.4 Å. Whereas, the local structure of liquid Sn looks more similar to the  $\beta$ -Sn

than the  $\alpha$ -Sn. The former has the body centered tetragonal structure with bond length of about 3.1 Å, while the latter has the diamond structure with the bond length of about 2.8 Å. The solid Sb has the rhombohedral structure, in which the local octahedra have bond lengths of 2.9 and 3.3 Å and the tetrahedra have the atomic distance of about 4.3 Å, roughly corresponding to the main peak and the shoulder on the  $G(r)$  curve of liquid Sb.

#### 2. Bond angle distribution

The bond angle distribution (BAD) function is a commonly used parameter to describe the nearest neighbor three-body relationship. It defines the angle formed by three neighboring atoms  $i$ ,  $k$ , and  $j$  under a certain cutoff, with  $i$  as the vertex.  $g(\theta)$  represents the probability of the angle  $\theta$  appearing, as expressed in Eq. (3):

$$g(\theta) = \frac{1}{\sum_{i=1}^N N_i(N_i - 1)} \sum_{i=1}^N \sum_{j=1}^{N_i} \sum_{k=j+1}^{N_i} \delta(\theta - \theta_{ijk}), \quad (3)$$

where  $\theta_{ijk}$  represents the angle between three atoms with  $i$  as the vertex. Figure 5 shows the bond angle distribution in these three liquids with the cutoff = 4.5, 4.7, and 5.4 Å, respectively, and consistent with the results reported in the previous literature [35,37,47]. Liquid In and Sn have obvious peak positions near 60° and 109°, being generally considered as the characteristics of the tetrahedral structure and the diamond structure. The appearance of bond angles around 60° and 90° for liquid Sb indicates the existence of tetrahedral and half-octahedral structures, respectively. It is worth noting that the peak intensity of tetrahedral in liquid In and Sn decreases sharply with increasing temperature. In contrast, the bond angle distribution for the tetrahedral structure exhibits

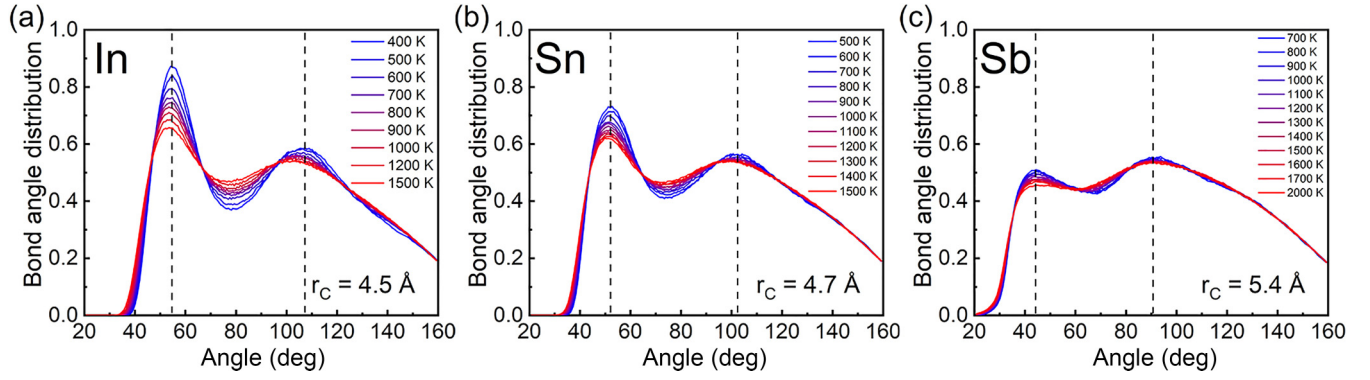


FIG. 5. Bond angle distribution calculated by using the configurations produced by AIMD simulations for liquid In (a), Sn (b), and Sb (c) with the cutoff = 4.5, 4.7, and 5.4 Å, corresponding to the first minimum positions in  $G(r)$  of their own, respectively.

only a small change in intensity, but a large change for the half-octahedral structure in liquid Sb. We also calculated the BAD with a cutoff of 3.8 Å corresponding to the right-side position of the first peak in  $G(r)$  of liquid Sb (see Fig. S9). The obtained shape of characteristic peaks further confirms the above data. The first peak shifting from 60° in Fig. S9 to a small angle direction in Fig. 5 could be due to the appearance of some long bond lengths with increasing cutoff.

### 3. Tetrahedral analyses

The bond angle distribution function implies the existence of a large number of tetrahedra in three metallic liquids, which is also consistent with the crystalline phases in Fig. 4 and previous reports [35,37,63–65]. On this basis, we calculated the number of tetrahedra in the liquid and defined the average number of tetrahedra contributed by each atom in the AIMD model under a certain truncation of bond length with a certain distortion tolerance. The distortion tolerance ( $dt$ ) is defined as Eq. (4):

$$dt = \frac{r_{\max} - r_{\min}}{r_{\max}} * 100\%, \quad (4)$$

where  $r_{\max}$  and  $r_{\min}$  stand for the longest and shortest bond lengths of a tetrahedron, respectively. Figure 6 shows the number and distribution of tetrahedra at  $dt = 30\%$  as the function of temperature, where the cutoff is 4.5 Å for liquid In and Sn, and 5.4 Å for liquid Sb. From Fig. 6(a), it can be found that the number of tetrahedra rescaled by atoms in three metallic liquids decreases with an increase of temperature. The liquid Sb exhibits two peak positions, reflecting a complex liquid phase structure [66]. We plotted the distribution of average bond length of tetrahedra in three liquids, as shown in Figs. 6(b)–6(d). The average bond length of tetrahedra in liquid In and Sn is around 3.4 Å, while about 3.5 and 4.3 Å for liquid Sb, roughly corresponding to the main peak and the right shoulder on the  $G(r)$  curves. The decay of small distorted tetrahedra in liquid Sb corresponds to the reduction of the 90° peak in the BAD function, likely due to the collapse of the half-octahedral structure (forming four distorted tetrahedra) at high temperatures. This conclusion is also supported by the results calculated for  $dt = 20\%$  and  $dt = 40\%$  in Figs. S10 and S11, respectively.

### 4. Charge density distribution

Based on the results of AIMD, we presented the density of states and charge density distribution near the melting temperature. The density of states (see Fig. S12) indicate that the three metallic liquids behave as a metal in the studied temperature ranges instead of appearing as a metalloid-metal transition. As shown in Fig. 7, the charge density distribution of liquid Sb exhibits strong localization, while it becomes relatively nonlocalized in liquid In, and somehow falls in between in liquid Sn, indicating that the atoms in liquid Sb are more tightly bonded than in liquid In and Sn. We extracted the atomic arrangements in the marked region with high concentrated charge densities in liquid Sb as shown in Figs. 8(a) and 8(b). Figure 8(c) displays a distorted tetrahedron containing two kinds of average bond lengths roughly 3.0 and 4.3 Å, respectively, well consistent with the positions of the main peak and its right shoulder on the pair distribution function and the shells of Sb crystal in Fig. 4(c). In alloy systems, Gangopadhyay and Kelton proposed that the anomalous

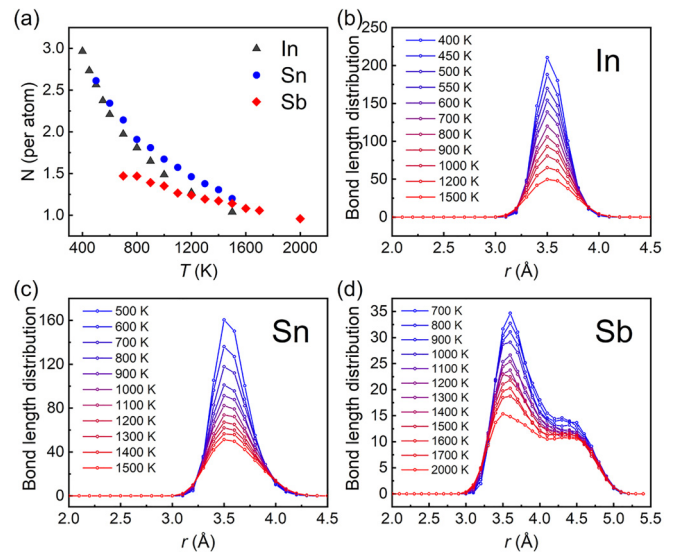


FIG. 6. (a) The average number of tetrahedra formed by each atom in liquid In, Sn, and Sb as a function of temperature. Distribution of tetrahedral bond lengths for liquid In (b), Sn (c), and Sb (d).

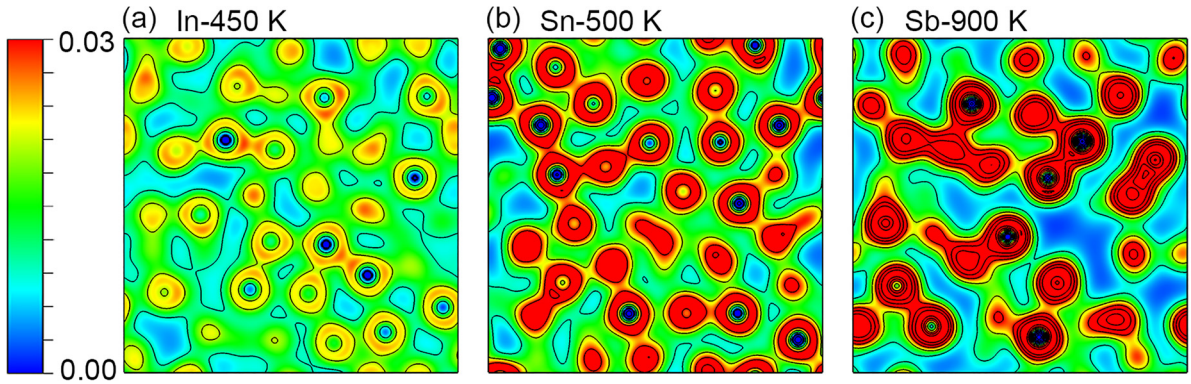


FIG. 7. Charge density distributions at melting point for liquid In (a), Sn (b), and Sb (c).

thermal behavior of the first peak in  $G(r)$  was ascribed to the temperature dependence of the various partial structure factors [67]. In single element systems, although there exists only one kind of atom pair, the bond length between atoms in the liquid state still has a wide distribution, as shown in the inset of Fig. 8(d). To probe different thermal responses of atom pairs, we traced the two points of the right and left edges at  $G(r) = 0$  of the main peaks shifting with temperature for three liquids. The two points show similar movements for liquid In and Sn, i.e., the right one shows expansion and the left shows contraction, as shown in Fig. 8(d). In contrast, for liquid Sb, the situation changes. The left point of liquid Sb shows contraction and the contraction coefficient is rather smaller than both liquid In and Sn. More anomalously, the right point undergoes not expansion but great contraction. It indicates that the atoms locating at 4.3 Å in the tetrahedra seem to be unstable and likely move close to the center atoms

as the temperature increases. The electronic structure of liquid Sb suggests that its structural evolution is quite different from that of liquid In and Sn due to the presence of both strong short bonds and weak long bonds. We also plotted the charge density distribution on other planes at  $1.6T_m$  and  $T_m + 500$  K in Fig. S13, further confirming the reliability of the conclusion deduced.

### 5. Atom sharing between clusters

Based on the Voronoi polyhedral analysis, we counted the number of atoms shared between two clusters, for which one means point sharing, two means line sharing, three means face sharing, and four or above means penetration of two clusters. The change of connection type  $\Delta S$  is defined as Eq. (5):

$$\Delta S^i = \frac{S_T^i - S_{T_m}^i}{S_{T_m}^i} \quad (i = 1, 2, 3, 3+) \quad (5)$$

when  $S_T^i$  represents the proportion of  $i$ -type connection between two clusters at temperature  $T$ , and  $T_m$  is the melting point. Figure 9 shows the  $\Delta S$  of three metallic liquids as a function of temperature. It is found that the number of cluster connections by sharing one or two atoms increases in liquid In and Sn while the three or above atom sharing decreases with rising temperature. Totally, the variation amplitude of different connections gets smaller from liquid In to liquid Sb. In particular, the bulk connection between clusters varies more significantly, showing the gradual deviation from the linear at a crossover temperature, well consistent with the coordination number changes (see Fig. S14).

### 6. Free volume analyses

The free volume, different from the cluster structure, just reflects the space or cavity among atoms. The calculation method is as follows: we used the configurations obtained from AIMD simulations, selected one atom, and set a Schmid radius to extract the volume out of the atoms. In our case, the Schmid radii of In, Sn, and Sb atoms are 1.63, 1.41, and 1.45, respectively. In addition, a rescaled factor, which is multiplied by the radius, was set to remove the free volume caused by small spaces among atoms. Figures 10(a)–10(c) show the three-dimensional distribution of the large-sized free volume near the melting points of metallic liquids with 1.4 times Schmid radius. Liquid In has small free volumes in a fragmented distribution, while liquid Sb shows large

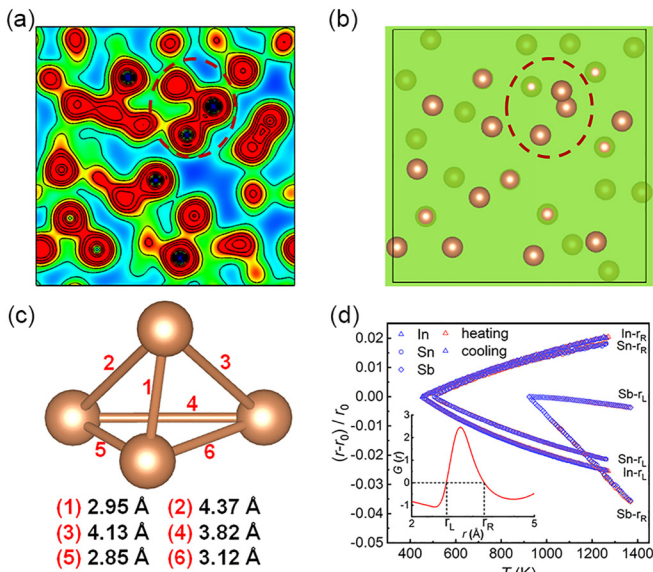


FIG. 8. (a) Projected charge density distributions in liquid Sb near the melting point. (b) Schematic diagram of the atomic arrangement corresponding to the charge distribution. (c) The detailed cluster structure marked in (b) by a red dashed circle. (d) Positions at the left and right sides of the main peak with  $G(r) = 0$  shifting with temperature.



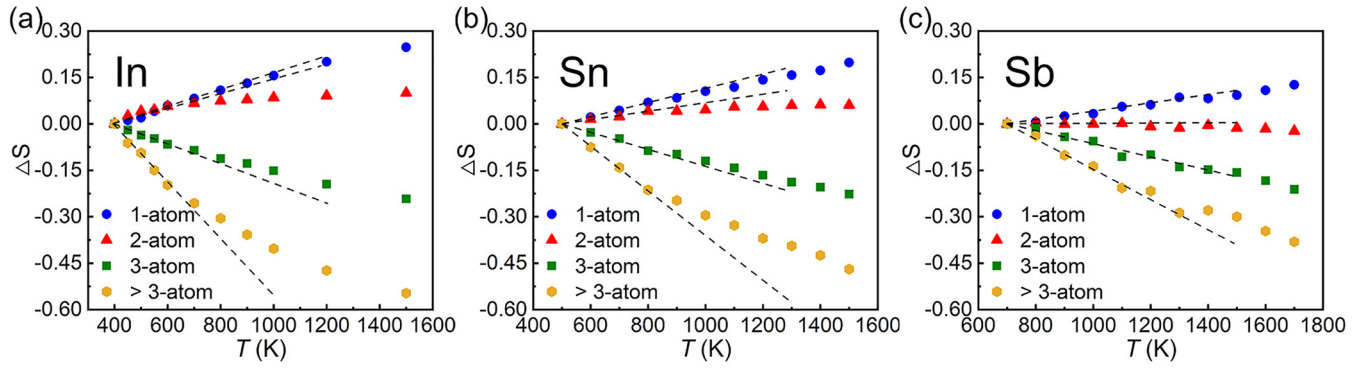


FIG. 9. Changes in cluster connection types as a function of temperature for liquid In (a), Sn (b), and Sb (c).

connected regions of free volume, and distribution in liquid Sn lies in between. We further calculated the distribution probability of free volume sizes at different temperatures, as shown in Figs. 10(d)–10(f). Liquid In has the most small-sized free volumes (below  $10 \text{ \AA}^3$ ), while liquid Sb has the largest large-sized free volumes (above  $20 \text{ \AA}^3$ ), and liquid Sn lies in between. With rising temperature, the free volumes increase in all three metallic liquids. In the case where the rescaled factor is 1, the average free volume as a function of temperature is shown in Fig. S15, indicating that the liquid Sb has the highest content free volume in three liquids. It means that the aggregation of solidlike regions and large-sized free volumes suggests the increased structure heterogeneity in liquid Sb, which is closely related with the anomalous peak shift observed in Figs. 2 and 3, making it different from that of liquid In and Sn.

The above results clearly reveal different temperature-dependent structural evolutions for liquid In, Sn, and liquid Sb. A viscosity jump of liquid In and Sn occurs around 700 K [27,28,38]. The sudden decrease in viscosity might be associated with the connection of clusters in the liquid, corresponding to a decrease in bulk and face connectivity and an increase in line and point connectivity. As shown in Fig. 9, the change in cluster connectivity of liquid Sb is obviously smaller than those of liquid In and Sn, consistent with the number of tetrahedral structure changes in three liquids. The structural inheritance of liquid Sb and the disappearance of Peierls distortion near 1023 K revealed by x-ray absorption fine structure spectra [46] further support our results that the liquid Sb changes its local atomic packing structure. The existence of greatly distorted tetrahedra in the liquid Sb, which have two different average bond lengths of about 3.3 and 4.3  $\text{\AA}$

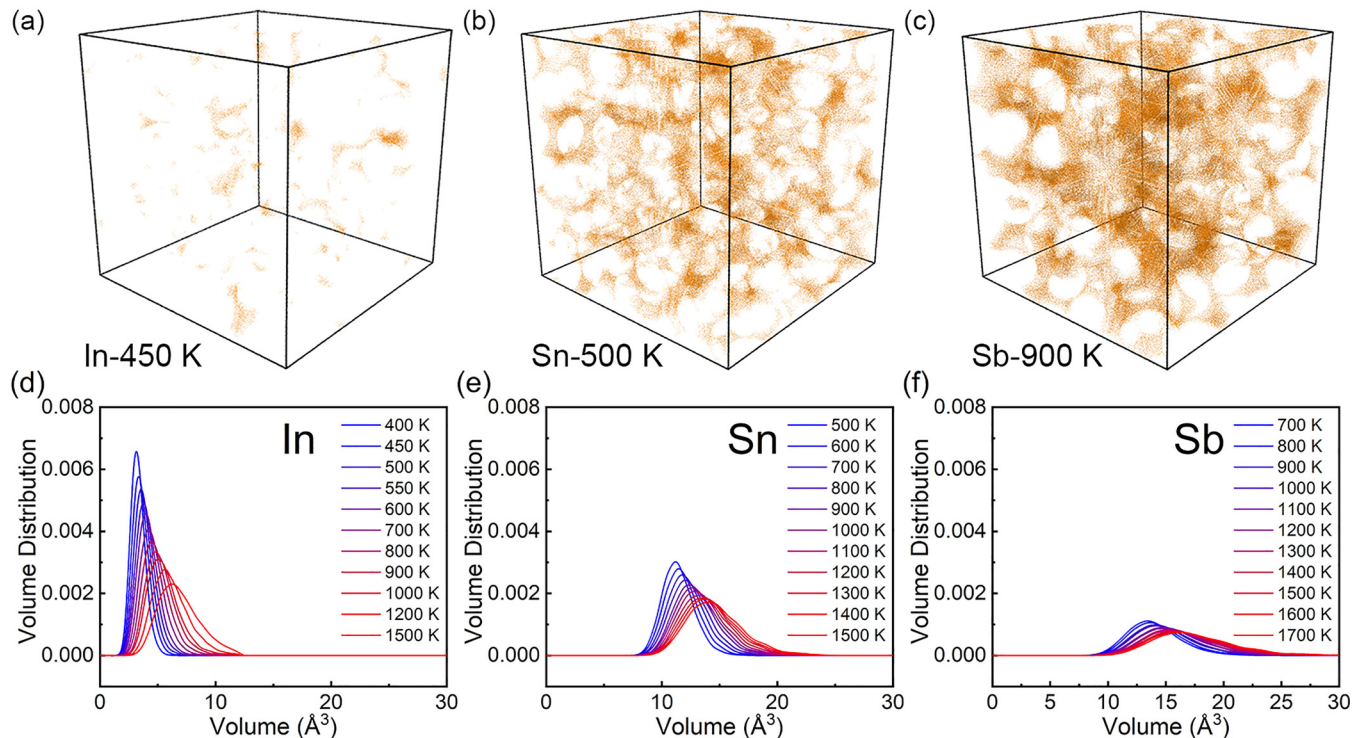


FIG. 10. Schematic diagrams of free volume distributions at melting point for liquid In (a), Sn (b), and Sb (c). The color indicates the position of the free volume. Free volume size distribution for liquid In (d), Sn (e), and Sb (f).



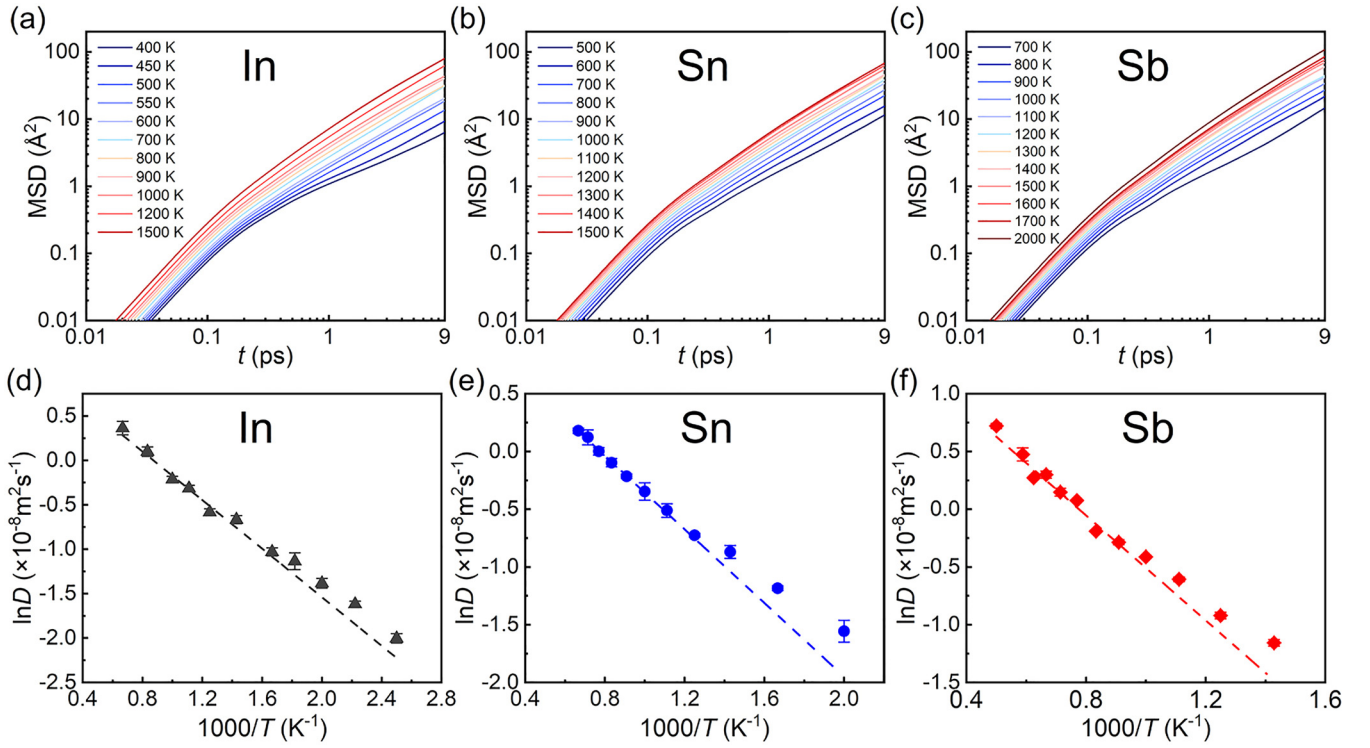


FIG. 11. Mean-squared displacement of liquid In (a), Sn (b), and Sb (c). Diffusion coefficient of liquid In (d), Sn (e), and Sb (f).

for Sb-Sb pairs within the first shell, may make the appearance of Peierls distortion. Solid Sb has the half-octahedral structure with one more atom locating in the center of the square, which could exist in the liquid [48], showing the  $90^\circ$  peak on the BAD curve. Theoretical calculations on tetrahedral bond strengths also confirm this view [65]. Different from liquid Sb, the BADs indicate that both tetrahedral and diamond structure could exist in liquid In and Sn. As such, liquid Sn was once proposed to have the mixed local structure of  $\alpha$ -Sn and  $\beta$ -Sn [37]. The temperature-dependent fractions of tetrahedral clusters and atom-sharing types obtained here strongly link with the structural evolutions in liquid In, Sn, and Sb. The anharmonicity due to the presence of two types of atom pairs with different bond lengths and the distinct aggregation of free volumes in liquid Sb are the essential reasons why its liquid structural evolution behavior is different from that of liquid In and Sn.

### C. Dynamical structure analyses by AIMD simulations

#### 1. Mean-squared displacement and self-diffusion coefficient

Dynamics strongly couple with local atomic packing structures. In dynamics, the mean-square displacement (MSD) is often used to characterize the dynamical behavior of atoms, as defined by Eq. (6):

$$\langle r^2(t) \rangle = \frac{1}{N} \left\langle \sum_{i=1}^N |r_i(t) - r_i(0)|^2 \right\rangle, \quad (6)$$

where  $N$  is the total number of atoms in the system, and  $r_i(t)$  and  $r_i(0)$  are the spatial positions of atoms  $i$  at time  $t$  and 0.

The diffusion coefficient of the system can be calculated by MSD using the formula as Eq. (7):

$$D = \lim_{t \rightarrow \infty} \frac{1}{6t} \langle r^2(t) \rangle. \quad (7)$$

Figure 11 shows the MSD and self-diffusion coefficient of atoms in three metallic liquids. Within 0.3 ps, the trajectory of atoms shows the ballistic motion, which may be thought of as the effect of lateral phonons [40]. Afterwards, the atomic behavior corresponds to the diffusive motion. From high to low temperature, the diffusion coefficient gradually deviates from the Arrhenius relationship, suggesting the existence of a potential crossover at the kink points within the studied temperature ranges. The relationship of the large diffusion activation energy at high temperatures is also confirmed by classic MD calculations for liquid In and Sn as well as the  $r^2$ scan meta-GGA for liquid Sb (see Figs. S16 and S17 in the Supplemental Material). This anomaly is likely a result of the strengthening of covalent interactions in metallic liquids at high temperatures, as reported in [42]. In strong glass-forming liquids [22], the deviation from the Arrhenius law means the breakdown of the Stokes-Einstein relation when the temperature is below  $T_A$ , at which the locally preferred structures start to form. Analogous to the  $T_A$  temperature, here we clearly reveal that the local atomic packing structures, such as tetrahedral clusters in their solid states, are indeed retained in the liquid In, Sn, and Sb. Above the crossover temperature, the number of tetrahedra, cluster connection, large-sized free volume, and anharmonicity of bond lengths have gradually become different from those of the low-temperature liquids.

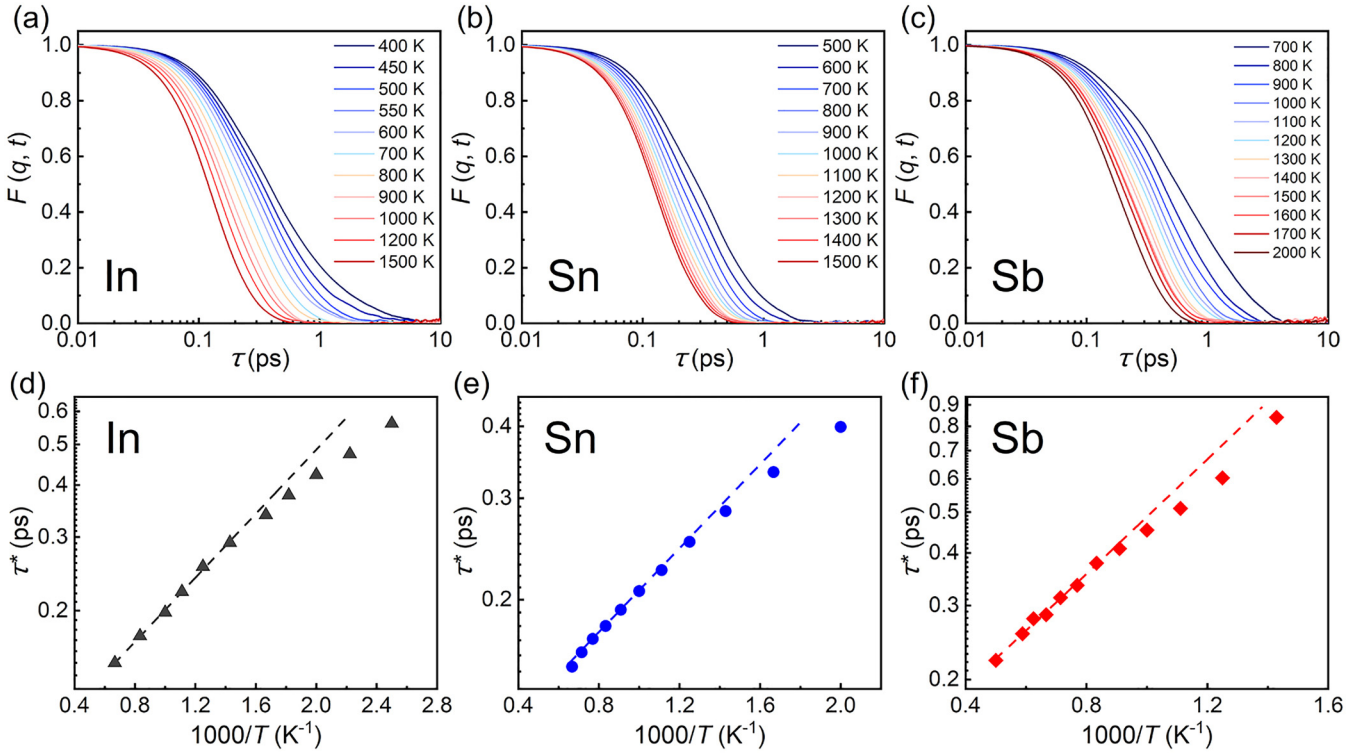


FIG. 12. Self-intermediate scattering function of liquid In (a), Sn (b), and Sb (c). Relaxation time extracted as the ISF decays to  $1/e$  under each selected temperature for liquid In (d), Sn (e), and Sb (f).

## 2. Intermediate scattering function

Intermediate scattering function (ISF) is often used to estimate the relaxation time and dynamical behavior in liquid systems, which can be obtained by taking the Fourier transform of the Van Hove correlation function, as presented in Eq. (8):

$$F(q, t) = \frac{1}{N} \left\langle \sum_j^N \exp\{-iq[r_j(t) - r_j(0)]\} \right\rangle, \quad (8)$$

where  $r_j(t)$  represents the position of the particle in the system at time  $t$ , and  $q$  is the first maximum position of the main peak of  $S(q)$ . We can estimate the structural relaxation time of three metallic liquids by calculating the self-intermediate scattering function,  $F(q, t)$ . Figure 12 shows the  $F(q, t)$  curves decay in an approximately exponential mode and take long time to zero as the temperature decreases. We define the  $\alpha$  relaxation time when the  $F(q, t)$  decays to  $1/e$  at each temperature. Figures 12(d)–12(f) show the relationship between  $\tau_\alpha$  and  $1000/T$  in the three studied systems. From the  $F(q, t)$ , one can see that the relaxation time can be well defined within the present waiting time, which is almost not affected by further extension of the waiting time. Different from the dynamic observation of MSD on the time window larger than 1 ps, the dynamic behavior within 1 ps could be related to the short-lived phonon behavior existing in the metallic liquids [29,40,49]. Similarly, the relaxation time at low temperatures less than the predication of the Arrhenius law is well consistent with the low diffusion activation energy in this temperature region. With the calculation of  $F(q, t)$  and analysis

of the relaxation time, different dynamical behaviors appear at the kink points, revealing the existence of a continuous but nonlinear structural evolution in three studied metallic liquids.

## 3. Non-Gaussian parameters

A non-Gaussian parameter (NGP) is often used to characterize the dynamical inhomogeneity of liquids and is defined as Eq. (9):

$$\alpha_2(t) = \frac{3\langle r^4(t) \rangle}{5\langle r^2(t) \rangle^2} - 1. \quad (9)$$

When the NGP is a large positive value, the  $r^2(t)$  of each particle has a large difference, reflecting the strong dynamical heterogeneity in the system. When the NGP value approaches 0, the particles in space obey the Brownian motion. When all the particles in the system vibrate in the same direction, the NGP takes the theoretical minimum value of  $-0.4$ . Figure 13 shows that the NGP parameter is close to 0 at the small  $t$  due to the ballistic motion of atoms in the cages, showing a state of Brownian motion. As time increases, the system enters a relaxed state and the NGP begins to increase, which means that the dynamical heterogeneity of the system increases during the relaxation. At high temperatures, the relaxation process starts earlier and ends faster with relatively small dynamical heterogeneity, showing the NGP is still not zero. Unlike the one peak feature of liquids reported in literature [68,69], the NGP curves of liquid In, Sn, and Sb showed two characteristic peaks at around 0.3 and 1.5–2.0 ps, similar with the NGP images of liquid Al [21]. With increasing temperature, the fast-moving peaks at 0.3 ps increase significantly but

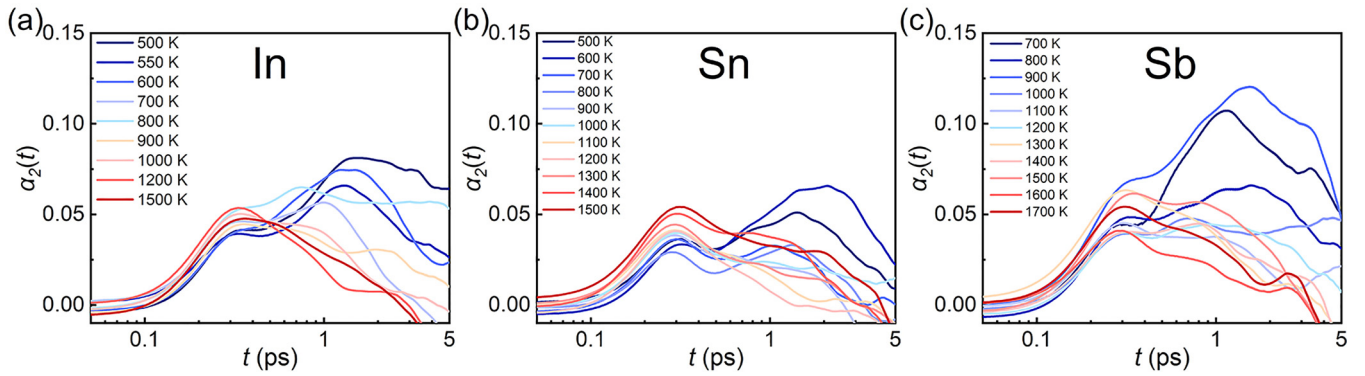


FIG. 13. Non-Gaussian parameter of liquid In (a), Sn (b), and Sb (c) produced by AIMD simulations, showing two peaks at about 0.3 and 1.5–2 ps, respectively, due to the presence of two kinds of dynamical heterogeneities.

their positions change little. This could be due to phonons arising from the strong anharmonicity in the amorphous structure [70,71]. The presence of two atomic pairs at different average distances in liquid Sb introduces a more complex chemical environment as well as stronger anharmonicity with the appearance of strong covalent bonds, which directly result in different dynamic characteristics. The slow-moving peaks decay rapidly in both intensity and position. It implies that a temperature-dependent transition of two dynamical modes exists in the liquids, somehow originating from their static structures, i.e., the tight packing of clusters could slow down the atomic dynamics whereas the loose packing ones could accelerate them. Atoms in the configurations produced by AIMD simulations are limited, which restricts obtaining the high-quality NGP data using a few atoms. Thus, we also calculated the NGP for liquid In and Sn with existing MEAM potentials by using the classical MD simulations (see Fig. S18 in the Supplemental Material). The results obtained from classical MD simulations show that the variation trends of NGP for liquid In and Sn are quite similar with those in Fig. 13 based on AIMD simulations, confirming the reliability of the results deduced from AIMD configurations.

#### IV. CONCLUSIONS

In this work, we systematically investigated the progressive polymorphic structural crossover in three In, Sn, and Sb metallic liquids through high-energy *in situ* synchrotron radiation XRD and AIMD simulations and obtained the following conclusions:

(1) We clearly observed a reversible and gradual structural crossover in liquid In, Sn, and Sb by analyzing position shifts of the first three main peaks on the  $S(q)$  and  $G(r)$  curves. However, the structural evolutions in liquid In and Sn are similar, but different from that in liquid Sb.

(2) Based on simulation results, we analyzed the bond angle distribution, number of tetrahedra, cluster connection,

diffusion coefficient, relaxation time, and non-Gaussian parameter, etc., by which we also observed the gradual structural crossovers in three studied metallic liquids.

(3) In liquid In and Sn, the structural crossover is closely related to the changes in tetrahedra and cluster connections. The clusters in liquid In and Sn are tightly connected at low temperatures and become looser at high temperatures. However, it mainly depends on the collapse of the octahedral structure in liquid Sb which inherits the solid-state structure of Sb until the crossover temperature. The short bonds are retained but long bonds get short in liquid Sb with temperature increasing, causing the atoms and free volume to be more aggregated on large scales than in liquid In and Sn.

(4) From the dynamics point of view, the increasing structural complexity of liquid In, Sn, and Sb, such as the appearance of covalent bonds and two average bond lengths in liquid Sb, the strong anharmonicity may cause their dynamic differences.

(5) This discovery of structural crossover in liquid In, Sn, and Sb can further contribute to the understanding of the liquid-liquid phase transition and structural evolution present in other metallic liquids.

#### ACKNOWLEDGMENTS

The authors acknowledge financial support from the National Natural Science Foundation (NNSC) of China (Grants No. 11975202, No. 12275237, and No. 52271156) and the NSC of Zhejiang Province (LZ20E010002), and the Fundamental Research Funds for the Central Universities. This research is also supported by the beamline 11-ID-C at APS, a U.S. Department of Energy (DOE) Office of Science user facility operated for the DOE Office of Science by Argonne National Laboratory under Contract No. DE-AC02-06CH11357. The HPC resources at National Supercomputer Center provided by Beijing PARATERA Tech Co., Ltd [72] are also gratefully acknowledged.

[1] S. Sastry and C. Austen Angell, *Nat. Mater.* **2**, 739 (2003).

[2] N. Jakse and A. Pasturel, *Phys. Rev. Lett.* **99**, 205702 (2007).

[3] S. Pascarelli, S. DePanfilis, and T. Neisius, *Phys. Rev. B* **62**, 3717 (2000).

[4] K. Tsuji, T. Hattori, T. Mori, T. Kinoshita, T. Narushima, and N. Funamori, *J. Phys.: Condens. Matter* **16**, S989 (2004).

[5] X. D. Wang and J. Z. Jiang, *Adv. Mater.* **29**, 1703136 (2017).

[6] T. Bryk, S. DePanfilis, F. A. Gorelli, E. Gregoryanz, M. Krisch,



- G. Ruocco, M. Santoro, T. Scopigno, and A. P. Seitsonen, *Phys. Rev. Lett.* **111**, 077801 (2013).
- [7] A. Cadien, Q. Y. Hu, Y. Meng, Y. Q. Cheng, M. W. Chen, J. F. Shu, H. K. Mao, and H. W. Sheng, *Phys. Rev. Lett.* **110**, 125503 (2013).
- [8] D. A. Carvajal Jara, M. Fontana Michelin, A. Antonelli, and M. de Koning, *J. Chem. Phys.* **130**, 221101 (2009).
- [9] R. Li, G. Sun, and L. Xu, *J. Chem. Phys.* **145**, 054506 (2016).
- [10] L. H. Xiong, X. D. Wang, Q. Yu, H. Zhang, F. Zhang, Y. Sun, Q. P. Cao, H. L. Xie, T. Q. Xiao, D. X. Zhang, C. Z. Wang, K. M. Ho, Y. Ren, and J. Z. Jiang, *Acta Mater.* **128**, 304 (2017).
- [11] Q. Yu, X. D. Wang, Y. Su, Q. P. Cao, Y. Ren, D. X. Zhang, and J. Z. Jiang, *Phys. Rev. B* **95**, 224203 (2017).
- [12] Y. Su, X. D. Wang, Y. Ren, Q. P. Cao, D. X. Zhang, and J. Z. Jiang, *Phys. Rev. B* **102**, 224103 (2020).
- [13] X. Chen, Q. Yu, Y. Su, X. D. Wang, Q. P. Cao, D. X. Zhang, and J. Z. Jiang, *Scr. Mater.* **148**, 68 (2018).
- [14] W. Xu, M. T. Sandor, Y. Yu, H. B. Ke, H. P. Zhang, M. Z. Li, W. H. Wang, L. Liu, and Y. Wu, *Nat. Commun.* **6**, 7696 (2015).
- [15] S. Lan, Y. Ren, X. Y. Wei, B. Wang, E. P. Gilbert, T. Shibayama, S. Watanabe, M. Ohnuma, and X. L. Wang, *Nat. Commun.* **8**, 14679 (2017).
- [16] S. Wei, F. Yang, J. Bednarcik, I. Kaban, O. Shuleshova, A. Meyer, and R. Busch, *Nat. Commun.* **4**, 2083 (2013).
- [17] H. B. Lou, X. D. Wang, Q. P. Cao, D. X. Zhang, J. Zhang, T. Hu, H. K. Mao, and J. Z. Jiang, *Proc. Natl. Acad. Sci. USA* **110**, 10068 (2013).
- [18] W. B. Zhang, X. D. Wang, Q. P. Cao, D. X. Zhang, and J. Z. Jiang, *J. Phys. Chem. B* **123**, 7055 (2019).
- [19] T. D. Xu, X.-D. Wang, E. M. Dufresne, Y. Ren, Q. P. Cao, D. X. Zhang, and J.-Z. Jiang, *Mater. Today Phys.* **17**, 100351 (2021).
- [20] K. Georarakis, L. Hennem, G. A. Evangelakis, J. Antonowicz, G. B. Bokas, V. Honkimaki, A. Bytchkov, M. W. Chen, and A. R. Yavari, *Acta Mater.* **87**, 174 (2015).
- [21] A. Jaiswal, T. Egami, and Y. Zhang, *Phys. Rev. B* **91**, 134204 (2015).
- [22] A. Jaiswal, T. Egami, K. F. Kelton, K. S. Schweizer, and Y. Zhang, *Phys. Rev. Lett.* **117**, 205701 (2016).
- [23] D. Kivelson, S. A. Kivelson, X. Zhao, Z. Nussinov, and G. Tarjus, *Phys. A (Amsterdam, Neth.)* **219**, 27 (1995).
- [24] D. Kivelson, G. Tarjus, X. Zhao, and S. A. Kivelson, *Phys. Rev. E* **53**, 751 (1996).
- [25] H. Ocken and C. N. J. Wagner, *Phys. Rev.* **149**, 122 (1966).
- [26] G. Y. Shen, N. Sata, N. Taberlet, M. Newville, M. L. Rivers, and S. R. Sutton, *J. Phys.: Condens. Matter* **14**, 10533 (2002).
- [27] S. J. Cheng, X. F. Bian, J. X. Zhang, X. B. Qin, and Z. H. Wang, *Mater. Lett.* **57**, 4191 (2003).
- [28] L. Wang, X. F. Bian, and J. T. Liu, *Phys. Lett. A* **326**, 429 (2004).
- [29] B. Wehinger, M. Krisch, and H. Reichert, *New J. Phys.* **13**, 023021 (2011).
- [30] S. Mudry, I. Shtablayvi, and U. Liudkevych, *Phys. Chem. Liq.* **55**, 254 (2016).
- [31] D. Jovic and I. Padureanu, *J. Phys. C: Solid State Phys.* **9**, 1135 (1976).
- [32] V. Petkov and G. Yunchov, *J. Phys.: Condens. Matter* **6**, 10885 (1994).
- [33] D. Cicco, *Phys. Rev. B* **53**, 6174 (1996).
- [34] S. Hosokawa, J. Greif, F. Demmel, and W. C. Pilgrim, *Chem. Phys.* **292**, 253 (2003).
- [35] T. Itami, S. Munejiri, T. Masaki, H. Aoki, Y. Ishii, T. Kamiyama, Y. Senda, F. Shimojo, and K. Hoshino, *Phys. Rev. B* **67**, 064201 (2003).
- [36] Y. Q. Wang, Y. Q. Wu, and X. F. Bian, *Chin. Phys. Lett.* **24**, 7 (2007).
- [37] L. Calderin, D. J. Gonzalez, L. E. Gonzalez, and J. M. Lopez, *J. Chem. Phys.* **129**, 194506 (2008).
- [38] Z. X. Yang, H. R. Geng, and N. Zhang, *Adv. Mater. Res.* **123**, 931 (2010).
- [39] Z. X. Yang, H. R. Geng, and N. Zhang, *Adv. Mater. Res.* **306–307**, 451 (2011).
- [40] S. Hosokawa, S. Munejiri, M. Inui, Y. Kajihara, W. C. Pilgrim, Y. Ohmasa, S. Tsutsui, A. Q. Baron, F. Shimojo, and K. Hoshino, *J. Phys.: Condens. Matter* **25**, 112101 (2013).
- [41] M. Mayo, S. Shor, E. Yahel, and G. Makov, *J. Chem. Phys.* **142**, 194501 (2015).
- [42] L. Xu, Z. Wang, J. Chen, S. Chen, W. Yang, Y. Ren, X. Zuo, J. Zeng, Q. Wu, and H. Sheng, *Nat. Commun.* **13**, 126 (2022).
- [43] E. Canessa, D. F. Mariani, and J. Vignolo, *Phys. Status Solidi B* **126**, K1 (1984).
- [44] Q. Wang, K. Q. Lu, and Y. X. Li, *Chin. Sci. Bull.* **46**, 1431 (2001).
- [45] L. W. Wang, Q. Wang, A. P. Xian, and K. Q. Lu, *J. Phys.: Condens. Matter* **15**, 777 (2003).
- [46] Q. Wang, C. X. Li, Z. H. Wu, L. W. Wang, X. J. Niu, W. S. Yan, Y. N. Xie, S. Q. Wei, and K. Q. Lu, *J. Chem. Phys.* **128**, 224501 (2008).
- [47] Q. H. Hao, Y. D. Li, X. S. Kong, and C. S. Liu, *Int. J. Mod. Phys. B* **27**, 1350012 (2013).
- [48] R. O. Jones, O. Ahlstedt, J. Akola, and M. Ropo, *J. Chem. Phys.* **146**, 194502 (2017).
- [49] M. Inui, Y. Kajihara, S. Hosokawa, A. Chiba, Y. Nakajima, K. Matsuda, J. R. Stellhorn, T. Hagiya, D. Ishikawa, H. Uchiyama, S. Tsutsui, and A. Q. R. Baron, *J. Phys.: Condens. Matter* **33**, 475101 (2021).
- [50] A. P. Hammersley, S. O. Svensson, M. Hanfland, A. N. Fitch, and D. Hausermann, *High Press. Res.* **14**, 235 (1996).
- [51] X. Qiu, J. W. Thompson, and S. J. L. Billinge, *J. Appl. Crystallogr.* **37**, 678 (2004).
- [52] B. H. Toby and R. B. Von Dreele, *J. Appl. Crystallogr.* **46**, 544 (2013).
- [53] G. Kresse and J. Furthmüller, *Phys. Rev. B* **54**, 11169 (1996).
- [54] S. Nosé, *J. Chem. Phys.* **81**, 511 (1984).
- [55] W. G. Hoover, *Phys. Rev. A* **31**, 1695 (1985).
- [56] P. E. Blochl, *Phys. Rev. B* **50**, 17953 (1994).
- [57] J. P. Perdew, K. Burke, and M. Ernzerhof, *Phys. Rev. Lett.* **77**, 3865 (1996).
- [58] J. W. Furness, A. D. Kaplan, J. Ning, J. P. Perdew, and J. Sun, *J. Phys. Chem. Lett.* **11**, 8208 (2020).
- [59] M. W. Terban and S. J. L. Billinge, *Chem. Rev.* **122**, 1208 (2022).
- [60] See Supplemental Material at <http://link.aps.org/supplemental/10.1103/PhysRevB.109.024112> for detailed information about the heating process of  $S(q)$  and  $G(r)$  of HEXRD,  $S(q)$  and  $G(r)$  of AIMD, centroids analyses, bond angle distribution with the cutoff of the first minimum in  $G(r)$ , tetrahedral analyses with different dt, and non-Gaussian parameter in MD simulations. The model and dynamic results obtained by the r2scan

- functional and classic MD are also provided to validate the reliability of the PBE functional.
- [61] M. I. Ojovan and D. V. Louzguine-Luzgin, *J Phys. Chem. B* **124**, 3186 (2020).
- [62] S. Lan, M. Blodgett, K. F. Kelton, J. L. Ma, J. Fan, and X.-L. Wang, *Appl. Phys. Lett.* **108**, 211907 (2016).
- [63] K. Sattler, J. Mühlbach, and E. Recknagel, *Phys. Rev. Lett.* **45**, 821 (1980).
- [64] C. Brechignac, M. Broyer, P. Cahuzac, M. de Frutos, P. Labastie, and J. P. Roux, *Phys. Rev. Lett.* **67**, 1222 (1991).
- [65] V. Sundararajan and V. Kumar, *J. Chem. Phys.* **102**, 9631 (1995).
- [66] T. Bryk, I. M. Ilenkov, and A. P. Seitsonen, *J. Phys.: Condens. Matter* **35**, 154003 (2023).
- [67] A. K. Gangopadhyay and K. F. Kelton, *J. Chem. Phys.* **148**, 204509 (2018).
- [68] H. Zhang, C. Zhong, J. F. Douglas, X. Wang, Q. Cao, D. Zhang, and J. Z. Jiang, *J. Chem. Phys.* **142**, 164506 (2015).
- [69] T. D. Xu, X. D. Wang, H. Zhang, Q. P. Cao, D. X. Zhang, and J. Z. Jiang, *J. Chem. Phys.* **147**, 144503 (2017).
- [70] H. E. Fischer, F. J. Bermejo, G. J. Cuello, M. T. Fernandez-Diaz, J. Dawidowski, M. A. González, H. Schober, and M. Jimenez-Ruiz, *Phys. Rev. Lett.* **82**, 1193 (1999).
- [71] P. Bordat, F. Affouard, M. Descamps, and K. L. Ngai, *Phys. Rev. Lett.* **93**, 105502 (2004).
- [72] <https://paratera.com/>.